Available online at www.sciencedirect.com
SCIENCE DIRECT®
Journal of the European Ceramic Society 25 (2005) 1015–1024
www.elsevier.com/locate/jeurceramsoc

Stress distribution in biomorphous SiC-ceramics under radial tensile loading

Tobias Fey, Heino Sieber, Peter Greil*

Department of Materials Science, Glass and Ceramics, University of Erlangen-Nuernberg, Martensstr. 5, Erlangen D-91058, Germany

Received 5 March 2004; received in revised form 3 May 2004; accepted 15 May 2004
Available online 22 July 2004

Abstract

Biomorphous SiC-ceramics were prepared by reactive Si-vapor infiltration of carbonized wood templates. The meso- and macroscopic anatomy of *pinus silv.* was converted into a highly porous, single-phase SiC-ceramic with elongated pore structure and anisotropic mechanical properties. The local stress distributions in the biomorphous ceramic subjected to external tensile loading were analyzed for different wood tissue anatomies using the Finite Element Method (FEM). First, the microscopical cellular morphology of the biomorphous SiC-ceramics was simulated by idealized two-dimensional substructures. The influence of the porosity, pore shape and strut thickness on the local stress distribution for radial (non-axial) load was investigated. Second, the stress distribution of the mesoscopical combined structure with the early wood/late wood transition was evaluated.

Keywords: Biomorphous SiC; Finite Element Method; Stress distribution; SiC

1. Introduction

Native plant structures exhibit a complex, hierarchically built anatomy, developed and optimized in a long-term genetic evolution process. The heterogeneous tissue of wood is formed by different cell types, with the structural features ranging from the micro (cell walls) to the macro scale (growth ring patterns).[1] The morphology and the arrangement of the different cells may vary in a wide range between the different kinds of wood with large vessel cells dominating in hard wood and tracheids dominating in soft wood. The open porosity is accessible for liquid or gaseous infiltration and may be as high as 70% in pine and down to 20% in ebony.[2] The diameter of the vessels and tracheids (named as pores) varies between 5 and 50 μm in softwood and between 1 and 300 μm in hard wood. Cells extending in radial direction (rays) and pits in the cell walls provide transportation paths perpendicular to the growth direction. In the living plant, the open pore system serves as a transport system for water and nutrition supply. Due to their hierarchically designed porous morphology, biological plant materials exhibit unique structure–mechanical property relationships such as a high flexibility and strength at low density.

Native plant structures have become of interest for advanced processing concepts of porous engineering ceramics in the recent years.[1–5] Homogeneous as well as heterogeneous cellular ceramics are of interest for applications such as micro filter in food processing, catalyst carrier in exhaust gas purification, high-temperature nozzle elements or micro-reactor devices.[6] The unidirected pore structure of wood (Fig. 1) with a strut thickness at the micrometer level cannot be reproduced by any conventional (foam, extrusion or substitution) ceramic processing technique so far.[2,4] The conversion of bioorganic structures by fast, high-temperature physio-chemical reaction routes into ceramic and composite materials with a meso- and macrostructure pseudomorphous to the natural template, can be readily achieved by means of biotemplating techniques.[2,4,6] The inherent open porosity in the natural plant is easily accessible for gaseous or liquid infiltration and subsequent reaction of the infiltrant with the template material to high-temperature resistant ceramic phases.[7–9]

Several biotemplating techniques for conversion of naturally grown wood into biomorphous SiC-based ceramics

* Corresponding author. Tel.: +49 9131 852 7543; fax: +49 9131 852 8311.
E-mail address: greil@ww.uni-erlangen.de (P. Greil).

0955-2219/$ – see front matter © 2004 Elsevier Ltd. All rights reserved.
doi:10.1016/j.jeurceramsoc.2004.05.008

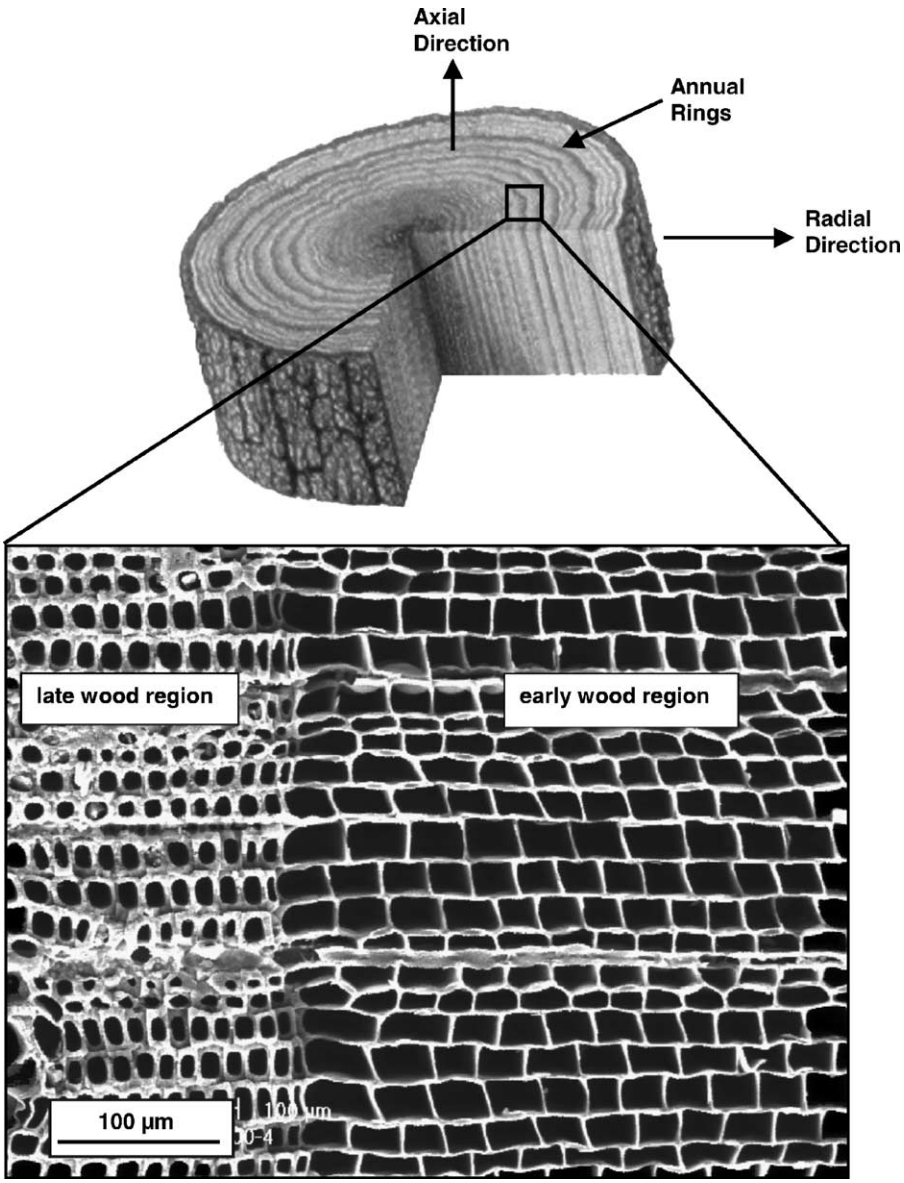

Fig. 1. SEM micrograph: axial cross section of pine wood-derived SiC-ceramic.

and composites were examined including reactive Si-melt or Si-vapor phase infiltration.[2,4–10] The conversion of native plant structures into SiC-based ceramics generally followed a two-step procedure. In a first step, a bio carbon template structure was prepared from solid wood by pyrolysis in inert atmosphere at temperatures above 400 °C. At this temperature the major biopolymer constituents of the cell wall material (cellulose, hemi cellulose and lignin) have decomposed into carbon. After pyrolysis, the cell walls of the native wood are converted into carbon struts with a thickness of a few micrometers or less. Details of the processing scheme, the properties of the bio carbon template, the dimensional changes and the weight loss during pyrolysis were described in Refs. 2,5,6. Subsequently, the carbonized bio carbon template was infiltrated at temperatures between 1450 and 1600 °C with liquid Si to form SiSiC-ceramic composites. Highly porous, single-phase SiC-ceramics were prepared by infiltration of a gaseous Si-precursor such as Si, SiO or CH_3SiCl_3.[7–11] The biomorphous SiC-based ceramics maintained the morphology of the biological template down to the submicrometer range and contained an unique directed pore morphology on the micrometer level.[2,4–11]

Due to the unidirected pore morphology, the highly porous, biomorphous SiC-ceramics prepared by Si-vapor phase conversion exhibit an anisotropic mechanical behavior with fracture stress in axial direction being 20 times higher compared to strength in radial direction.[11–13] The strength in axial direction mainly depends on the material fraction on the axial cross section similar to the strength of honeycombs.[1] In contrast, strength in radial direction strongly depends on cell morphology features, which include shape, size and topology of pores and struts. Generally, the

in-plane stiffness and strength (stress acting perpendicular to cell elongation) are the lowest, because *in-plane* loading makes the cell walls bend. The *out-of-plane* stiffness and strength (stress acting parallel to cell elongation) are much larger because they require axial extension or compression of the cell walls. With increasing fractional density cell walls (e.g. the struts) increase in average thickness but cell shape can change significantly and hence stiffness and strength increase in a complex manner.

Because of seasonal variation of growth conditions growth ring patterns develop with low density/high porosity in the early and high density/low porosity in the late wood region. As a consequence, non-linear transitions of material properties (Young's modulus, toughness, strength) are expected to affect the fracture behavior in radial direction.[12–14] The influence of the porosity on the mechanical properties of highly porous cellular ceramics was described by several authors.[15–18] Numerical Finite Element Methods (FEM) were applied to simulate the stress distribution in ceramic honeycomb structures[19] and the effect of pore shape on Young's moduli and Poisson's ratio.[20–22] An overview about the use of FEM simulations for ceramics is given by Mackerle.[23]

The aim of the present work is to estimate the stress distribution of cellular biomorphous ceramics subjected to fictive *in-plane* loading situations. Focus is set on the variation of hierarchical structure features such as cell shape and density distribution. The calculations were conducted for SiC pseudomorphous to pine wood as a representative biomorphous ceramic. In a first step, the microstructure was characterized. A geometric algorithm that generates a simplified model of the complex morphology of biomorphous ceramics on the two different hierarchical levels of the wood cell system and the seasonal ring pattern was developed. Pine wood exhibits a relative uniform pore morphology with square and elliptical pore shapes and a pronounced early wood/late wood transition. In a second step the cellular structure was separated into idealized substructures composed of square and elliptical shaped pores. Finally, the substructures were combined in a complex model, which to a first approximation, represents the natural tissue anatomy in the late wood/early wood transition region. All structures were subjected to radial tensile loading and the stress distributions were calculated by variation of structural parameters.

2. Experimental procedure

Pine wood (*Pinus silvestris*) is a coniferous soft wood with a rather uniform microstructure. It consists of 90–95 vol.% tracheids, which are long and slender cells tapered at the ends. The size of the tracheids (diameter up to 50 μm, length up to few millimeters[24]) depends on the growth conditions such as changing temperature or water supply. Specimens of pine wood were pyrolysed in nitrogen atmosphere at 800 °C for 4 h resulting in complete decomposition of organic material to carbon, tar and volatile products like CO_2, CO, CH_4. Despite an anisotropic shrinkage of 22.5% in axial direction and 27.7% in radial direction the initial tissue anatomy was kept unchanged in the carbon template. Subsequently, biomorphous SiC-ceramic was produced by Si-vapor infiltration at 1600 °C in Argon-atmosphere of ambient pressure. For further details of the processing see.[2,4–9] Fig. 1 shows the microstructure of pine wood-derived SiC-ceramics with a view in axial growth direction. The pine wood-derived SiC-ceramic is characterized by an open porosity of about 71% (geometric density ≈1 g/cm^3, skeleton density ≈3.1 g/cm^3). Strength measurements by four-point bending (20/40 mm) showed a pronounced anisotropy of the compression strength with 124 MPa in axial, but only 27–35 MPa in the radial and tangential directions.[6,10] The Young's modulus was found to vary between 7 and 20 GPa in axial and between 3 and 11 GPa in radial direction.[6]

For generation of the FE-model, the complex structure of the pine wood-derived SiC-ceramics with early- and late wood regions was divided into idealized substructures. The pore diameter d and strut thickness t describe each cell of the substructure for the simplest square and elliptical pore models. Experimental values for d and t were taken from the biomorphous SiC-ceramic and range from 5 to 30 μm for d and 1 to 5 μm for t. The fractional density ρ^* can be expressed by t and d as follows:[15]

$$\rho* = \frac{\rho}{\rho_s} = C_1 \frac{t}{d} \quad (1)$$

where C_1 depends on the cell shape ($C_1 = 4.17$ for square cells and $C_1 = 1.17$ for elliptical cell, determined by image analysis). ρ is the geometrical density of the porous compact and ρ_s is the strut density. Fig. 2 shows the radial distribution of ρ^* as determined experimentally by SEM image analysis. While in early wood region $\rho^* < 0.4$, a pronounced increase of ρ^* up to 0.9 was found to occur in late wood regions. The regular undulations of density are expected to give rise for radial variation of the local mechanical properties.

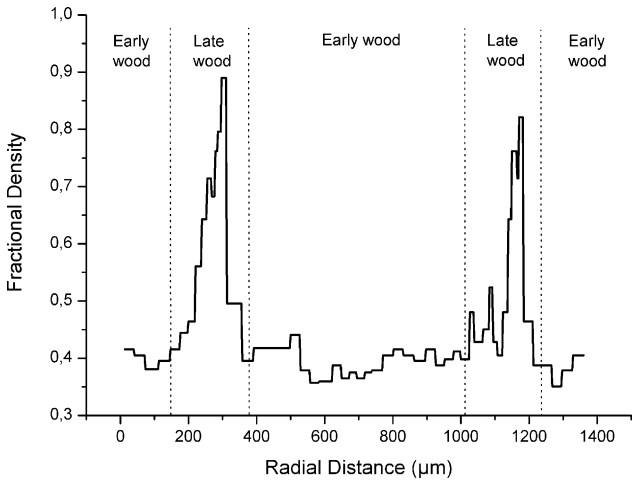

Fig. 2. Radial density distribution.

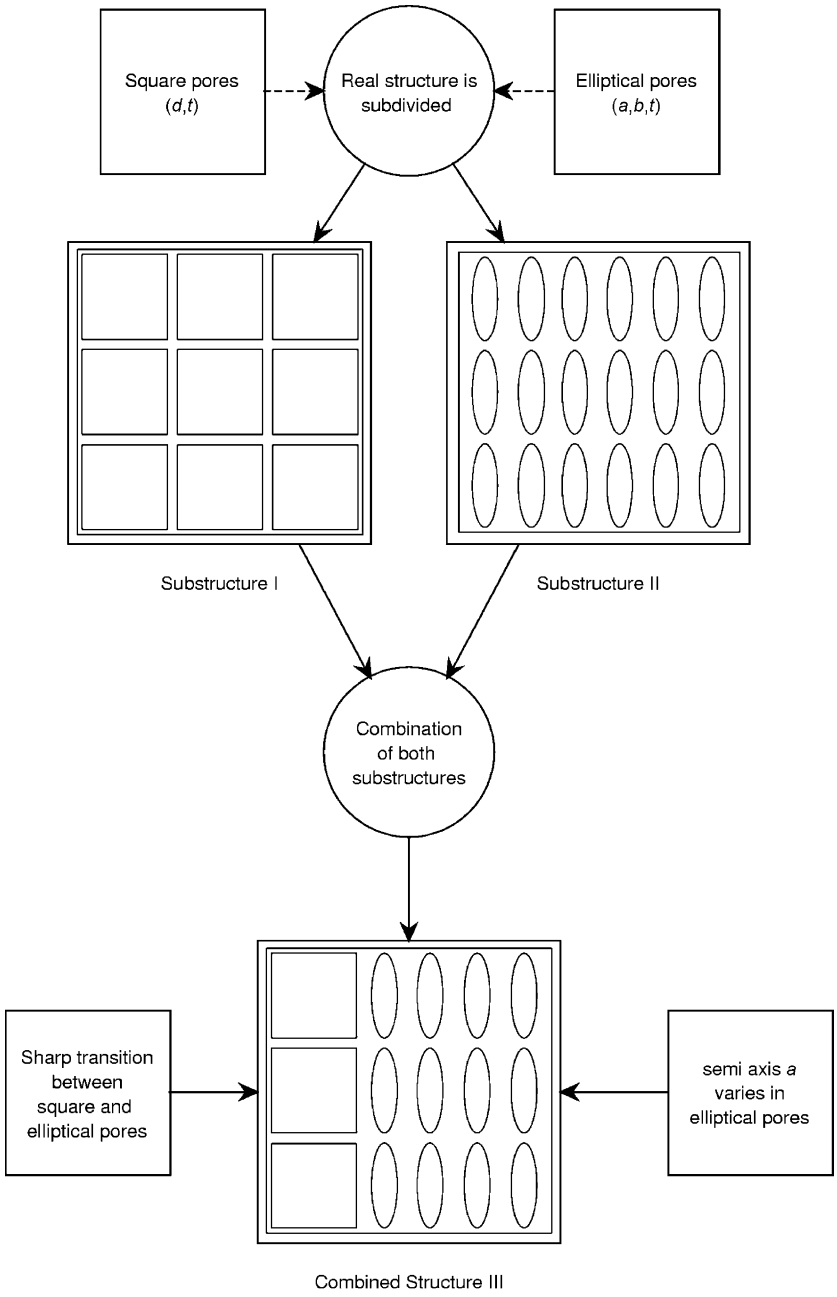

Fig. 3. Schematic flow chart for structure modeling.

The strategy of evaluation of complex cell arrangements by combining the simple models to a complex model is outlined in Fig. 3. The pore channels in the wood tissue were assumed to be continuous in *z*-direction (axial). According to a pine tracheid length of 1–6 mm[24] cell homogeneity in *z*-direction is supposed.

As a consequence, the cross section perpendicular to the axial direction is supposed to contain full information on the three-dimensional structure. For simplicity, all substructures were described as two-dimensional models. Each substructure consists of nine cells ($n = 9$) with each single cell containing one pore ($P1$). The cells are regularly arranged so that the structure model is characterized by a translation periodicity in *x*- and *y*-direction. Using a bottom-up method, the complex wood cell system was first divided into *substructure I* (square pores) (Fig. 4a) and *substructure II* which contains elliptical pores where the semi axis *a* varies from $0 < a < d$ (Fig. 5a). The complex structure with the early wood/late wood transition areas (*combined structure III*) (Fig. 6A) was derived by combination of *substructure I* and *substructure II* with linearly decreasing semi axis *a* for the elliptical pores. The properties of *combined structure III* will then be given as superposition of the initial substructure properties (Table 1).

Table 1
Substructure development

Substructure	Description	Algorithms to calculate pore coordinates (number of cells = n)
Substructure I	Cells with square pore shape	Calculating left lower vertex coordinates of square pore $0 < ix_1, iy_1 < n$ are cell numbers $x = t(ix_1 + 1) + ((d + t)ix_1)$ $y = t(iy_1 + 1) + ((d + t)iy_1)$
Substructure II	Cells with elliptical pore shape	Pore coordinates depend on semi axis a $x_{\text{elliptical}} = \left(\frac{a}{2} + t\right)(ix_2 + 1) + \left(\frac{a}{2} + t\right) ix_2$ $y_{\text{elliptical}} = \left(\frac{a}{2} + t_2\right)(iy_2 + 1) + \left(\frac{a}{2} + t\right) iy_2$
Substructure III	Cell length $l = 1$ mm and constant or variable length of semi pore axis a	Square pore coordinates are calculated in analogy to *substructure I* (ix_1 and iy_1 have to be adjusted). Elliptical pore coordinates ($x_{\text{elliptical}}$, $y_{\text{elliptical}}$) depend on square pore coordinates (x_{square}) and semi pore axis a. Strut size $t_2 = 2t$ $x_{\text{elliptical}} = \left(\frac{a}{2} + t_2\right)(ix_2 + 1) + \left(\frac{a}{2} + t_2\right) ix_2 + x_{\text{square}} + d + t$ $y_{\text{elliptical}} = \left(\frac{a}{2} + t_2\right)(iy_2 + 1) + \left(\frac{a}{2} + t\right) iy_2$ $a_{ix2+1} = a_{ix2} + q$ (gradient pore morphology)

The FE-calculations were applied to the substructure models using Marc 7.3.2 and Mentat 3.3.2 (MSC-Software).[25–27] The pore coordinates in the models were generated by PERL-programs. For the two-dimensional models marc element 125 (eight square node element with reduced integration)[26] were used. The strut material was represented by the material properties of β-SiC (Young's modulus 410 GPa; possion's ratio 0.14; density 3.1 g/cm^3).[28] The

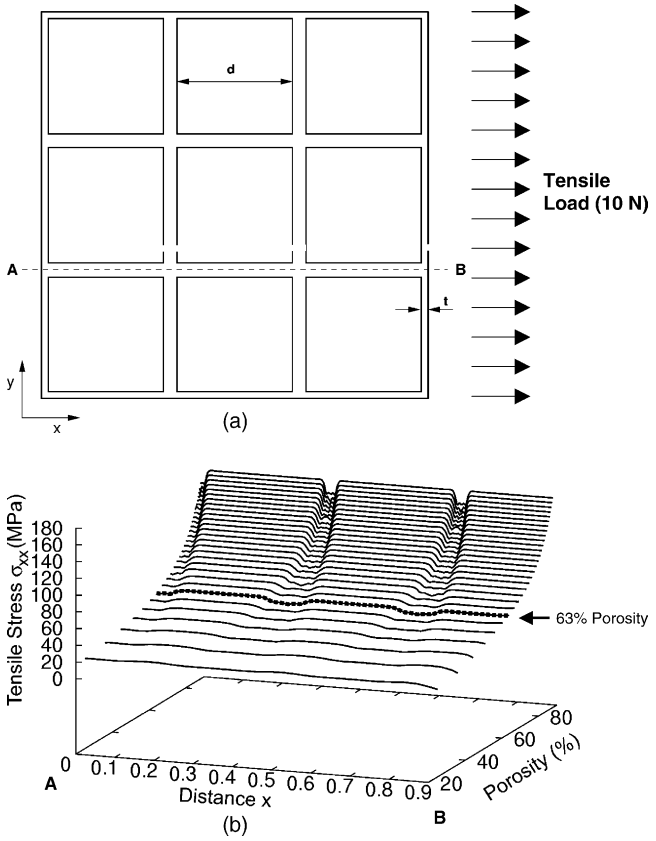

Fig. 4. *Substructure I*: (a) cell arrangement and (b) stress distribution under tensile loading.

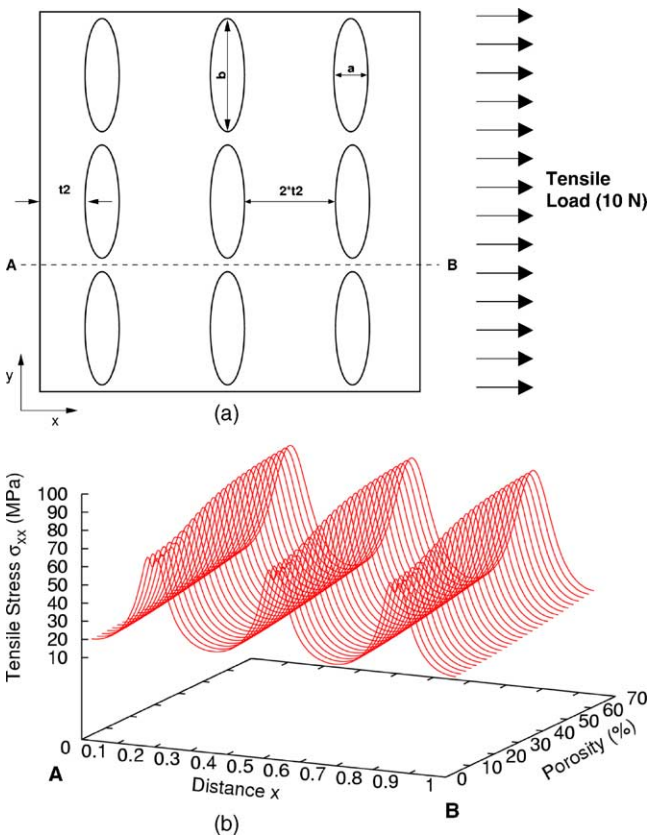

Fig. 5. *Substructure II*: (a) cell arrangement and (b) stress distribution under tensile loading.

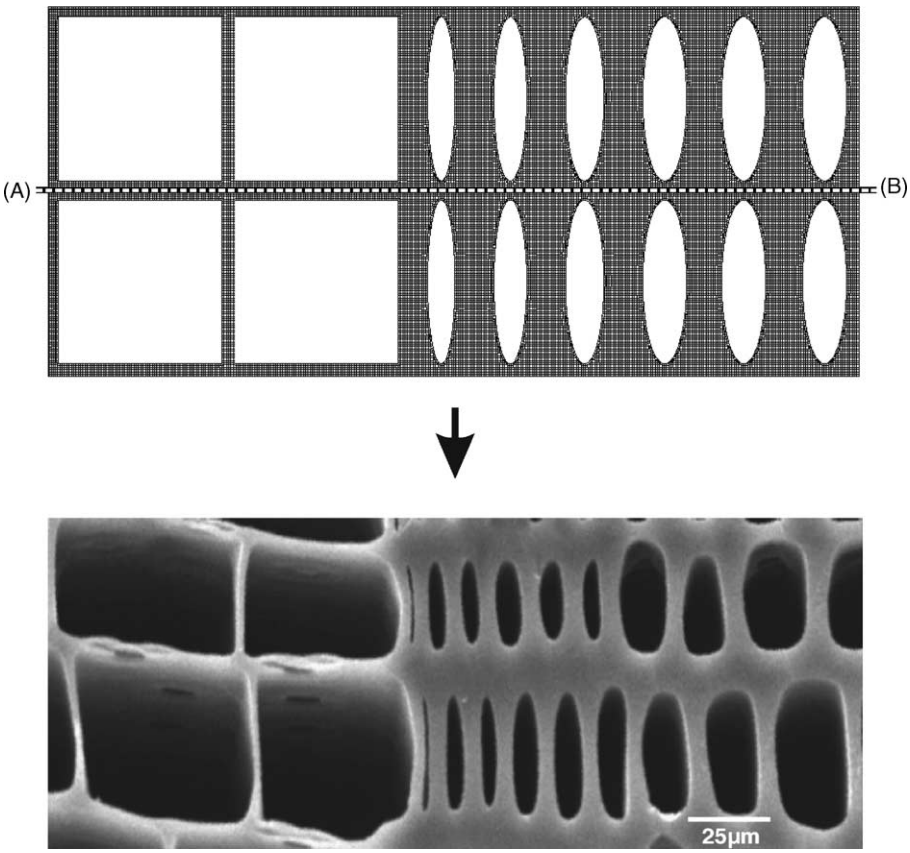

Fig. 6. Cell arrangement in combined structure III: combined structure model (top) and biocarbon template of pine wood.

two-dimensional models were applied to radial loading conditions (Figs. 5–7). The load was applied as tension stress. The following boundary conditions were applied:

- fixed nodal displacement for node $\in \{(0, y, z), (x, 0, y), (x, y, 0)\}$,
- tying for node $\in \{(x_{max}, y, z), (x, y_{max}, z), (x, y, z_{max})\}$ to retained node $(x_{max}, y_{max}, z_{max})$,
- for two-dimensional models edge load (10 N) on right outline.

Heterogeneity of the cellular material derived from natural template was taken into account by variation of structural parameters (strut thickness t, pore diameter d, and pore shape). The calculations of the two-dimensional models were done in plain strain mode ($\in_z = 0$).[28,29]

3. Results

3.1. Substructures I and II

Substructure I represents the early wood region in pine wood anatomy with square pores arranged in a regular manner as shown in Fig. 1. Fig. 4b shows the distribution of tensile stress component σ_{xx} in the struts of regularly arranged square cells (*substructure I*) subjected to an uniaxial tensile load of 10 MPa in radial direction. The porosity was varied from 20% to 90%. Fig. 4b presents the FEM-simulation of the stress distribution for a typical porosity of 63% found in the biomorphous SiC-ceramic. Compression stress state is observed in the vertical struts whereas the horizontal struts are subjected to tensile stresses, parallel to the loading direction. With increasing porosity the tensile stress in the struts parallel to the loading direction rises from approximately 20 MPa at a porosity of 20% to 170 MPa at 80%, respectively. At the strut crossings a reduced tensile stress is found, the difference to the remote strut region being increased with increasing porosity. This is to be expected because of decreasing strut thickness from 15 μm at 20% porosity to 2 μm at 80% porosity, respectively. When strut thickness varies over the length of strut ligament due to growth inhomogenities local stress intensification might be even higher than predicted (170 MPa compared to applied remote stress of 10 MPa) and may give rise for strut failure when the materials tensile strength is exceeded.

Fig. 5b shows the corresponding stress distribution in *substructure II* that is characterized by elliptical pore shape. The elliptical pores of *substructure II* were constructed by reducing the semi axis a. The arrangement of elliptical pores as given in Fig. 5a represents the cellular structure in the late wood regions of pine. Compared to the square pores tensile stresses accumulate at the top of the pores and give rise

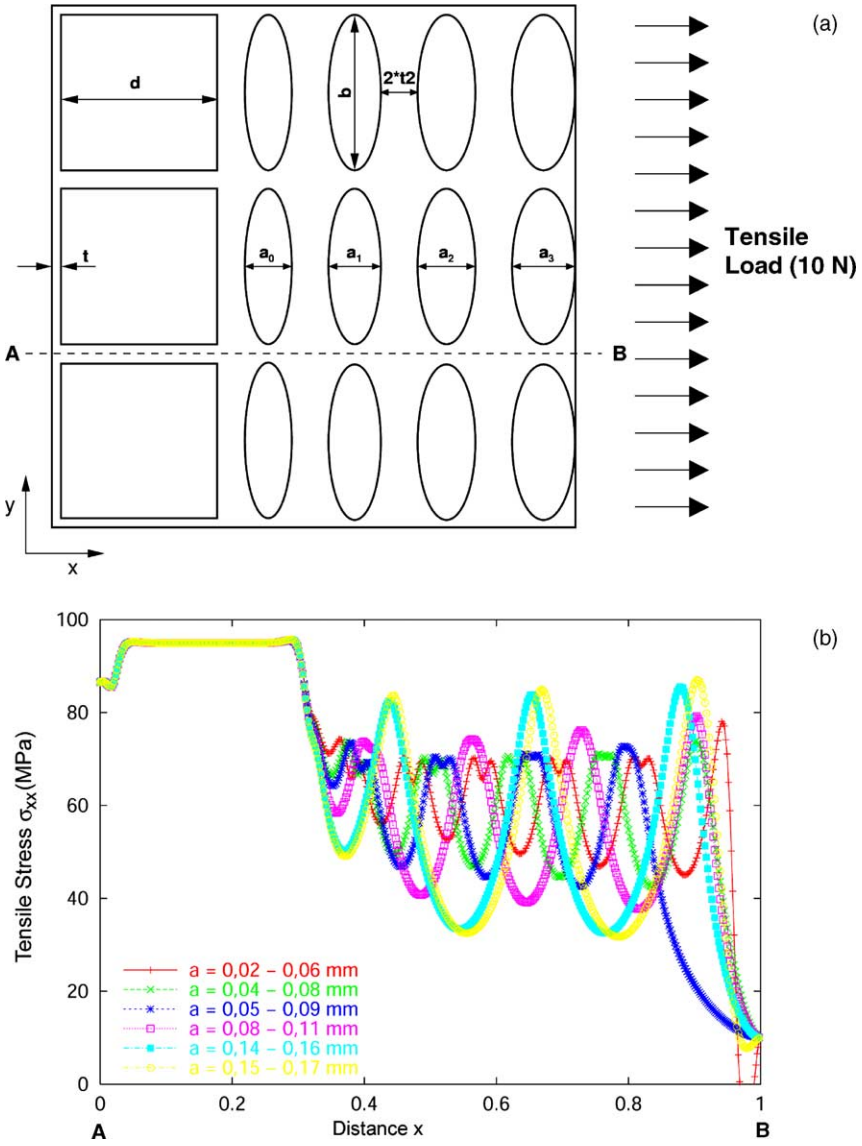

Fig. 7. *Combined structure III*: (a) cell arrangement and (b) stress distribution under tensile loading.

for pronounced stress singularities. The transformation of a single pore from round to elliptical has been analytically described by[28] and numerically by.[30] The FEM-simulations show, that the porosity of the structure is reduced for decreasing a and the maximum stress σ_{xx} increased accordingly.

3.2. Simulation of the seasonal ring pattern

3.2.1. Combined structure III

The extension from the individual substructures to a combined structure model which represents the early wood/late wood transition region is shown in Fig. 6. For comparison the real tissue structure of pine-derived SiC-ceramic in the early wood/late wood transition region is shown below.

To account for the radial variation of elliptical pore geometry, semi axis a was varied with increasing distance from the early wood/late wood boundary. The number of elliptical pores varied between three and four depending on the value of a_n (Fig. 7). The strut size t and pore diameter d of the square pores were fixed to match a porosity of 80% in the square cell region. The strut size in early wood/late wood interface was defined as $1.5t$ and, between the elliptical pores, as $2t$ in agreement with the experimental values. The average porosity of the combined structure model varied from 40% ($0.02\,\text{mm} < a_n < 0.06\,\text{mm}$) up to 60% ($0.15\,\text{mm} < a_n < 0.17\,\text{mm}$).

Generally, the maximum tensile stress σ_{xx}^{AB} in the late wood area (elliptical pores/low porosity) is lower than in the early wood area (square pores/high porosity). However, with increasing a the maximum tensile stress σ_{xx}^{AB} increases in the late wood area and reached approximately 100% of the tensile stress level in the early wood region when a equals d.

4. Discussion

4.1. Effect of porosity and pore shape

Assuming a constant reference cell length l ($l = 1$) with translational periodicity of cell arrangement the cellular channel porosity can be expressed as a function of either strut size t or pore diameter d for square pores:

$$P_{\text{square}} = \left(1 - \frac{2}{d/t + 2}\right)^2 \tag{2}$$

and for elliptical pores (special case semi axis $a = b$) as:

$$P_{\text{elliptical}} = \left(1 - \frac{2}{d/t + 2}\right)^2 \frac{\pi}{4}. \tag{3}$$

The FEM-simulation indicated that the calculated maximum tensile stress σ_{xx} for square(s) and elliptical(e) pores (special case $a = b$) depends in a linear relation on the d/t ratio by

$$\sigma_{xx} = A_{\text{square,elliptical}} \frac{d}{t} - B_{\text{square,elliptical}} \tag{4}$$

where A and B are geometric constants which account for the different substructures models ($A_{\text{square}} = 10.02172$, $A_{\text{elliptical}} = 10.03866$ and $B_{\text{square}} = -2.8 \times 10^{-4}$, $B_{\text{elliptical}} = -3.53551$). Fig. 8a shows the calculated tensile stress σ_{xx} as a function of the ratio d/t for different pore shapes. Accordingly, the tensile stress σ_{xx} can be related to the porosities by:

$$\sigma_{xx} = A_{\text{s,e}} \left(\frac{X_{\text{s,e}} 2\sqrt{P_{\text{s,e}}}}{1 - X_{\text{s,e}}\sqrt{P_{\text{s,e}}}} \right) - B_{\text{s,e}} \tag{5}$$

For the geometric constant X values of 1 (square) and $\pi/4$ (elliptical) were derived. Fig. 8b compares both the analytical relations (Eq. (5)) with the results of numerical stress

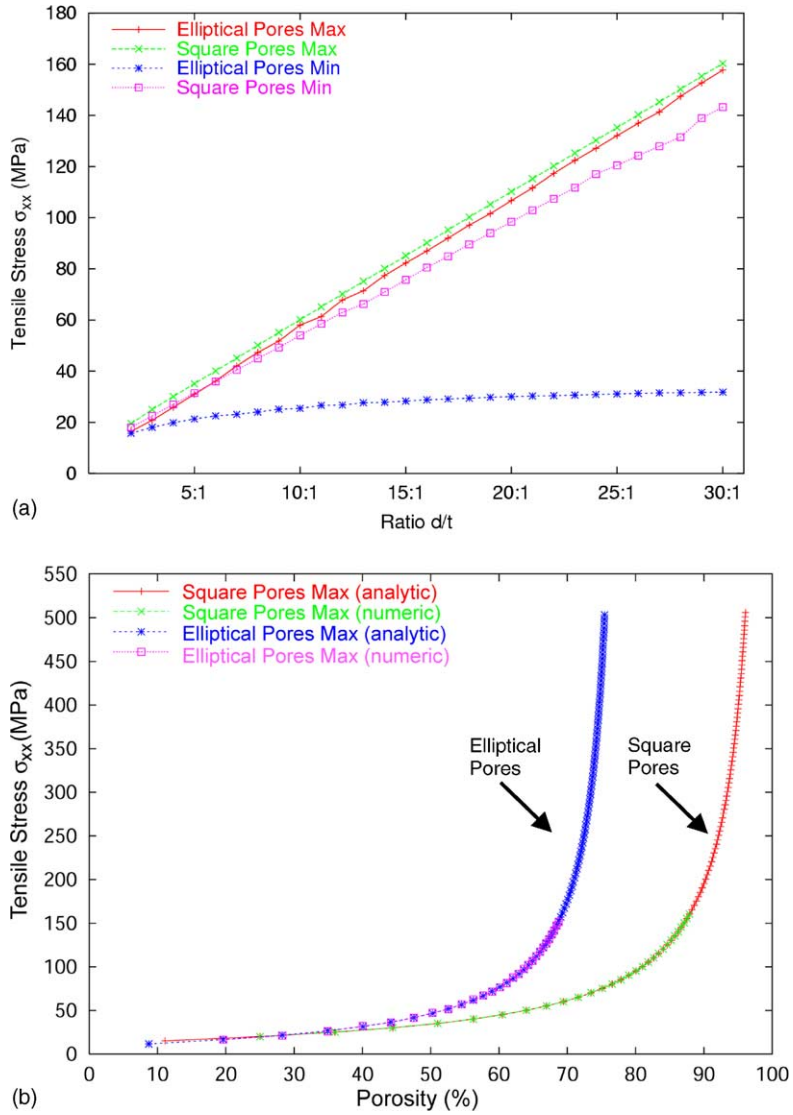

Fig. 8. Analytical model of maximum tensile stress (a) as a function of (a) the ratio d/t (Eq. (4)) and (b) porosity (Eq. (5)).

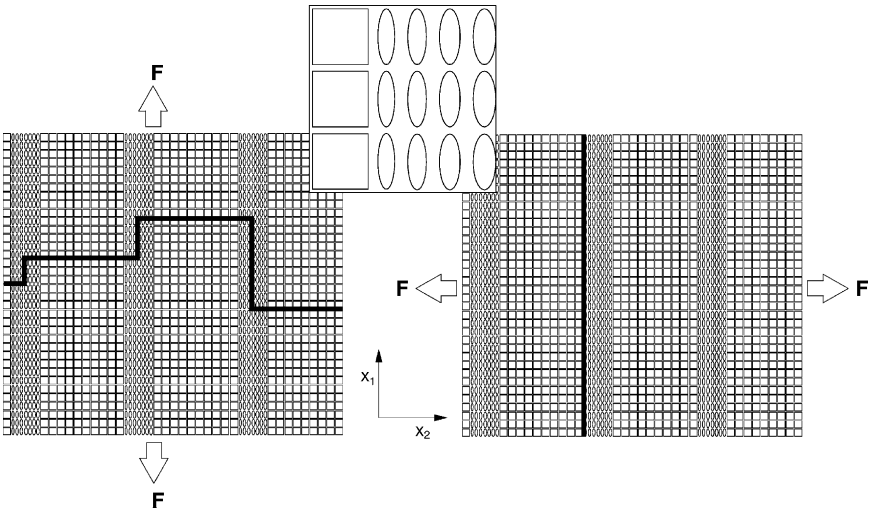

Fig. 9. Tentative crack propagation scheme of biomorphous ceramic.

analysis. The maximum tensile stress strongly increases with increasing porosity. The square cells exhibit a lower tensile stress at the same level of porosity compared to spherical pores. It is interesting to note, however, that the maximum tensile stress applied is similar for both idealized substructures for the same d/t ratio. The large increase of the maximum tensile stress for elliptical pores at high porosities compared to square pores is due to the much larger decrease in the minimum strut thickness t.

The seasonal ring patterns of pine primarily contain square pores in the early wood area and elliptical pores with different semi axis in the late wood area. For the analyzed range of semi axis $0.02\,\text{mm} < a_n < 0.17\,\text{mm}$, the maximum stress σ_{xx}^{AB} in the late wood area does not exceed σ_{xx}^{AB} in the early wood area. With increasing a_n, however, σ_{xx}^{AB} increases in the late wood area, too. The final stress distribution at the early wood/late wood transition area is the result of both parameters—porosity and pore shape. The influence on the maximum stress of each parameter can be determined by splitting the combined structure back into two parts for the different pores (early wood and late wood). The porosity of each part is named as *partial porosity*. The partial porosity δP_S for the early wood area (square pores) is 80% and was kept constant with increasing a_n. For the late wood area (elliptical pores) the partial porosity δP_E varies from 20% to 51% for a linear increase of a_n (step size 0.01) from 0.02 to 0.17 mm. The range of a_n was chosen in accordance to natural tissue anatomy of wood.

Analyzing the late wood area, the maximum of σ_{xx}^{AB} increased from 69 MPa ($\delta P_E = 20\%$) to 86 MPa ($\delta P_E = 51\%$) almost linearly with increasing partial porosity δP_E. To identify the dominating parameter, the resulting maximum stress $\sigma_{xx}^{AB\,(\text{late wood})}$ in the late wood area for different partial porosities has to be compared to the maximum stress in the early wood area $\sigma_{xx}^{AB\,(\text{early wood})}$. For the maximum $\delta P_E = 51\%$ the maximum stress $\sigma_{xx}^{AB\,(\text{late wood})}$ is 88% of $\sigma_{xx}^{AB\,(\text{late wood})}$. For the minimum $\delta P_E = 20\%$ the maximum stress $\sigma_{xx}^{AB\,(\text{late wood})}$ obtains 70% of $\sigma_{xx}^{AB\,(\text{late wood})}$. This marginal stress increment of only 18% is connected with a pronounced increase of δP_E of more than 250%.

Local variation of fracture toughness is expected to occur when the cell size, strut thickness and cell morphology are changed near the growth ring patterns. Thus, undulations of low and high-density regions (growth ring patterns and rays) are likely to affect crack propagation in the crack extension direction. For a reasonable Weibull modulus of 8, an increase of fracture toughness by 30% and of strength by 25% was estimated to be possible in a biomorphous SiC-ceramic.[12] Thus, the transition regions might act as crack deflection interfaces with the growth ring transitions cracking sequentially which gives rise for a series of step like drops in the stress–strain curve. Fig. 9 finally shows a schematic view of the crack propagation, which may occur depending on the loading conditions applied. Crack advance is likely to be localized on the highly stressed areas whereas regions of high density should yield higher fracture resistant segments in the loaded structure.

5. Conclusions

The stress distribution in biomorphous SiC-ceramics subjected to *in-plane* tension was calculated by FEM. The complex cellular structure of the early wood/late wood transition regions was described by a combination of idealized substructures composed of square and elliptical pore morphologies. For the idealized substructures, an analytical correlation between the porosity and the maximum stress was derived for the ratio between the pore diameter and the strut thickness. The stress distribution in the early wood/late wood transition was evaluated by superposition of the lower hierarchical levels (idealized substructures). The highest applied stress was found to occur in the square pore region due to the higher porosity. The regular undulations of early

wood/late wood regions account for periodical alternations of density and stress intensification which are supposed to cause non-planar crack propagation under specific loading conditions.

References

1. Gibson, L. J. and Ashby, M. F., Hierarchical cellular materials. *MRS Proc.* 1992, **295**.
2. Sieber, H., Hoffmann, C., Kaindl, A. and Greil, P., Biomorphic cellular ceramics. *Adv. Eng. Mater.* 2000, **2**(3), 105–109.
3. Ahsby, M. F. and Jones, D. R. H., *Engineering Materials 2 (An Introduction to Microstructures, Processing and Design)*. Pergamon Press, Oxford, 1986.
4. Greil, P., Biomorphous ceramics from lignocellulosics. *J. Eur. Ceram. Soc.* 2001, **21**, 105–111.
5. Byrne, C. E. and Nagle, D. E., Cellulose derived composites—a new method for materials processing. *Mater. Res. Innovat.* 1997, **1**, 137.
6. Greil, P., Lifka, T. and Kaindl, A., Biomorphic cellular silicon carbide ceramics from wood: I. Processing and microstructure. *J. Eur. Ceram. Soc.* 1998, **18**, 1961–1973.
7. Singh, M., Martínez-Fernández, J. and de Arellano-López, A.R., Environmentally conscious ceramics (ecoceramics) from natural wood precursors. *Curr. Opin. Solid State Mater. Sci.* 2003, **7**(3), 247–254.
8. Sieber, H., Vogli, E., Müller, F., Greil, P., Popovska, N. and Gerhard, H., CVI-R gas phase processing of porous, biomorphic SiC ceramics. *Key Eng. Mater.* 2002, **206–213**, 2013–2016.
9. Vogli, E., Sieber, H. and Greil, P., Biomorphic SiC-ceramic prepared by Si-gas phase infiltration of wood. *J. Eur. Ceram. Soc*. 2002, **22**, 2663–2668.
10. Vogli, E., Mukerji, J., Hoffmann, C., Kladny, R., Sieber, H. and Greil, P., Conversion of oak to cellular silicon carbide ceramic by gas-phase reaction with silicon monoxide. *J. Am. Ceram. Soc*. 2001, **84**, 1236–1240.
11. Ota, T., Takahashi, M., Hibi, T., Ozawa, M., Suzuki, S., Hikichi, Y. and Suzuki, H., Biomimetic process for producing SiC wood. *J. Am. Ceram. Soc.* 1995, **78**(12), 3409–3411.
12. Greil, P., Vogli, E., Fey, T., Bezold, A., Popovska, N., Gerhard, H. and Sieber, H., Effect of microstructure on the fracture behavior of biomorphic silicon carbide ceramics. *J. Eur. Ceram. Soc.* 2002, **22**, 2697–2707.
13. Martínez Fernández, J., Muñoz, A., de Arellano López, A.R., Valera Feria, F. M., Domínguez-Rodríguez, A. and Singh, M., Microstructure–mechanical properties correlation in siliconized silicon carbide ceramics. *Acta Mater.* 2003, **51**(11), 3259–3275.
14. Vogli, E., Sieber, H. and Greil, P., Wood derived porous and cellular ceramics. In *Ceramic Engineering and Science Proceedings, Vol 23 (4)*, ed. H.-T. Lin and M. Singh. The American Ceramic Society, 2002, pp. 211–218.
15. Gibson, L. J. and Ashby, M. F., *Cellular Solids: Structure and Properties (2nd ed.)*. Pergamon Press, Oxford, 1997.
16. Wagh, S., Sing, J. P. and Poeppel, R. B., Dependence of ceramic fracture properties on porosity. *J. Mater. Sci*. 1993, **28**, 3589–9353.
17. Boccaccini, A. R. and Fan, Z., A new approach for the Young's modulus-porosity correlation of ceramic materials. *Ceram. Int*. 1997, **23**, 239–245.
18. Rice, R. W., Monolitihic and composite ceramic machining flaw-microstructure-strength effects: model evaluation. *J. Eur. Ceram. Soc.* 2002, **22**, 1411–1424.
19. Winterstein, G., Stahn, M., Voigt, M. and Kuhn, G., Ceramic honeycumb structures. *CFI—Ceram. Forum Int.* 1998, **75**, 8–16.
20. Roberts, A. P. and Garboczi, E. J., Elastic properties of model porous ceramics. *J. Am. Ceram. Soc.* 2000, **83**, 3041–3048.
21. Ramakrishnan, N. and Arunachalam, V. S., Effective elastic moduli of porous ceramic materials. *J. Am. Ceram. Soc.* 1993, **76**.
22. Goto, K. and Kagawa, Y., Fracture behaviour and toughness of a plane-woven SiC fibre-reinforced SiC matrix composite. *Mater. Sci. Eng.* 1996, **A211**, 72–81.
23. Mackerle, J., Ceramics and ceramic matrix composites: finite element and boundary element analyses. A bibliography (1998–2000). *Finite Elem. Anal. Des.* 2002, **38**, 567–577.
24. Gibson, L. J., Wood: A natural fibre reinforced composite. *Metals Mater.* 1992, **8**, 333.
25. MSC-Software, *MSC. Marc Volume A: Theory and User Information*. MSC-Software, München, 2000.
26. MSC-Software, *MSC. Marc Volume B: Element Library*. MSC-Software, München, 2000.
27. MSC-Software, *MSC. Marc Volume C: Program Input*. MSC-Software, München, 2000.
28. Sawin, G. N., *Stress Intensification at Holes*. VEB Verlag Technik, Berlin, Germany, 1956 (in German).
29. Eschenauer, J. and Schnell, W., *Theory of Elasticity I*. B.I. Wissenschaftsverlag, Germany, 1986 (in German).
30. Schneider, T., *Modeling of Strength of Porous Ceramics*. Ph.D. thesis, University of Erlangen-Nuernberg, 2001 (in German).